Chapter 7
Future of Superhard Material Design, Processing and Manufacturing

Dr. Maweja Kasonde, CEng MIMMM
and Dr. Valentine Kanyanta, CEng MIMechE

Abstract Advancements in superhard and ultrahard material design will require a paradigm shift in the way we think about material design. It will need thinking outside the box and using unconventional technologies. The biggest challenges with superhard materials is their inherently lower fracture toughness, expensive to manufacture and difficult to process into final formats or geometries (such as for cutting tools) required by end users. These geometries are at times extremely complex 3D shapes with micron size features which are difficult to achieve via conventional processing methods. All these challenges limit the use of superhard and ultrahard materials in many drilling and machining applications. This chapter looks at firstly how the fracture toughness of superhard materials can be enhanced using concepts such as biomimicry, dispersing a tough phase in a superhard material matrix, engineering controlled defects, designing functionally graded structures, nanostructuring and imbedding a three-dimensionally interpenetrating network of a tough phase inside a brittle matrix. Secondly, the chapter briefly discusses additive manufacturing (e.g. 3D printing) as a route to reducing material waste/cost, increasing responsiveness to market needs for customised and complicated 3D shapes and eliminating the need for post-processing (i.e. moving towards a single-step manufacturing process).

1 Introduction

Superhard and ultrahard[1] materials such as cubic boron nitride and diamond have transformed the abrasive markets in terms of economics and productivity. Owing to their extremely high hardness, these materials are now widely used is industrial

[1] Diamond is the only intrinsically ultrahard material with a hardness of greater than 80 GPa, usually about 100 GPa. Superhard materials are defined as those with a load invariant Vickers hardness greater than 40GPa and ultrahard materials as having a hardness exceeding 80 GPa.

Dr. M. Kasonde, CEng MIMMM (✉)
Research Fellow, Element Six Limited, Oxfordshire, UK
e-mail: maweja.kasonde@e6.com

Dr. V. Kanyanta, CEng MIMechE
Principal Research Scientist, Element Six Limited, Oxfordshire, UK
e-mail: valentine.kanyanta@e6.com

V. Kanyanta (ed.), *Microstructure-Property Correlations for Hard, Superhard, and Ultrahard Materials*, DOI 10.1007/978-3-319-29291-5_7

applications requiring very high resistance to abrasion wear. They offer high material removal rates, superior surface finish and longer tool life. All these factors contribute to favourable economics of cutting, drilling and grinding operations. For example, the use of diamond-based cutting tools in oil and gas has resulted in significantly increased productivity and efficiency compared carbide and steel tools. The high penetration/drilling rates means drilling times can be significantly reduced. Long tool life also means less number of drill bit changes or trips (Scott 2006). These two factors have a significant impact on the cost per foot drilled, which includes both the direct and indirect overhead costs.

In cutting and machining operations, the ability to maintain a sharp cutting edge is extremely important in order to achieve superior surface finish of the work piece. This is made possible by the high resistance to abrasion wear of the cutting tool material. The tool also needs to be able to retain high hardness at elevated temperatures. At the cutting tip, temperatures can be extremely high especially in cases involving machining of super alloys such as INCONEL where temperatures are thought to be in excess of 1000 °C (Kennam et al. 2015). Diamond and cubic boron nitride have very good hot hardness and hence another reason why they are preferred in applications such as high speed turning of super alloys and case-hardened steels. The downside with these two superhard materials, especially in the case of diamond, is the low resistance to chemical wear when machining certain types of materials. Diamond-based cutting tools cannot be used to machine ferrous or iron-containing materials because of the high solubility of carbon in iron. This possesses significant restrictions on the type of materials which can be machined. Diamond also has poor thermal stability at temperatures above 600 °C under atmospheric pressure conditions (Westraadt et al. 2015). Above this temperature, it starts to transform into graphite which is a much softer phase. Cubic boron nitrides has relatively better thermal stability than diamond and can be used to machine ferrous materials (Goel et al. 2012). However, cubic boron nitride is not completely inert with iron during machining of ferrous alloys. Studies have shown that there is dissolution and diffusion of cBN into the flowing chip and work piece (Arsecularatne et al. 2005; Barry and Byrne 2001; Giménez et al. 2007; Narutaki and Yamane 1979; Zimmermann et al. 1997). Therefore it also does suffer from similar problems of chemical wear as diamond, although in the case of the former this is less pronounced. Improving resistance to chemical wear and thermal stability is necessary if these traditional materials are to find much wider applications as cutting tools.

The other challenge with traditional superhard materials, i.e. diamond and cubic boron nitride, is their inherently low fracture toughness. Although these materials are extremely hard and are widely employed as cutting tools in difficult to machine materials, their resistance to crack propagation (or fracture toughness) is only a few $MPa/m^{0.5}$. For polycrystalline diamond, the values of mode I fracture toughness is usually below 10 $MPa/m^{0.5}$ and can be as low as 5 $MPa/m^{0.5}$ depending on the average grain size of diamond particles, metal content and synthesis conditions (Droty et al. 1995; McNamara et al. 2015; Morrell et al. 2010; Petrovic et al. 2011). In the case of polycrystalline cubic boron nitride, values of between 8 and

14 MPa/m$^{0.5}$ have been reported (Carolan et al. 2013a). This is still far below what can be achieved with cemented carbides, i.e. up to 25 MPa/m$^{0.5}$ (Okamoto et al. 2005; Sandvik Hard 2005), and even an order of magnitude lower when compared to tool steels. The toughness of single crystal diamond or cubic boron nitride is even much lower.[2] Because of the low fracture toughness, diamond and cubic boron nitride materials are usually susceptible to unpredictable and catastrophic failure during application. Not only are such failures undesirable in terms of reduced productivity, they can cause significant damage to parts being machined and increase the scrap rate. As a result, the industry still needs superhard materials with much increased fracture toughness.

In addition to low fracture toughness, resistance to chemical wear and sometimes poor thermal stability, traditional superhard materials also present significant manufacturing challenges which involve high pressure and high temperatures usually in excess of 5 GPa and 1400 °C, respectively. Generating such conditions is an extremely expensive process. There is also a high level of complexity involved in designing press systems that can generate the required high pressure and temperature conditions. The current alternative manufacturing process to high pressure and high temperature (HPHT) is chemical vapour deposition (CVD). However, this is equally an expensive and energy-intensive process. Not only are these materials expensive to make, they are also difficult to process into final tool geometries required by end users. Therefore, there is also a requirement for making near net-shaped formats so that any secondary processing is kept to the minimum.

In order for diamond and cubic boron nitride to remain preferred superhard materials for cost-effective solutions in abrasive markets, the challenges highlighted above, i.e. low fracture toughness, resistance to chemical wear, thermal stability, manufacturing costs and difficulty of processing, need to be addressed. This chapter looks at possible solutions to overcoming some of these challenges.

2 Overcoming the Toughness Challenge

Enhancing the fracture toughness of materials which are inherently brittle is not trivial. Diamond and cubic boron nitride are intrinsically superhard because of the cubic crystal structure and short covalent bonds between their atoms. This structure offers very high resistance to plastic flow, and hence high hardness. However, the absence of plastic deformation is detrimental to the toughness of the material. As a result diamond and cubic boron nitrate are intrinsically brittle, with low fracture toughness or resistance to crack growth. The only way the toughness of these

[2] Polycrystalline materials have higher fracture toughness than single crystalline materials due to the random orientation of crystallographic planes. In single crystal materials, fracture always takes place along weaker planes (less energy barrier). By having fracture or slip planes randomly oriented as in a polycrystalline material, the resistance to crack propagation is enhanced.

materials can be enhanced is via extrinsic toughening mechanisms that inhabit crack growth or alter the way cracks propagate. In most cutting and drilling applications, diamond and cubic boron nitride materials are used in the form of sintered polycrystalline structures. Commercially available polycrystalline diamond (PCD) is prepared via a high pressure and high temperature liquid-phase sintering process. The result is an intergrown skeleton of diamond grains with metal inclusions occupying the interstices in the material. Intergrowth is made possible via the dissolution and reprecipitation of carbon atoms by using a metal solvent catalyst. On the other hand, polycrystalline cubic boron nitride consists of superhard particles (i.e. cubic boron nitride) bonded together by a binder phase and does not usually contain any intergrowth between the superhard particles. The preparation of these two materials is extensively covered in Chaps. 1 and 2.

There is always a requirement in industry for materials that are simultaneously superhard, strong and tough. However, the challenge in designing such materials is that toughness and strength are generally mutually exclusive, meaning enhancing one result in the other being sacrificed. This is also usually the case with toughness and hardness. Therefore, it is extremely difficult to improve the fracture toughness of these superhard materials without negatively affecting their hardness and strength. One way of defeating this toughness—strength (or hardness) conflict—is through biomimicry. Natural materials are known to achieve an excellent combination of strength and toughness (Chen et al. 2012; Karambelasa et al. 2013; Rabiei et al. 2010; Ritchie 2011; Sowmya et al. 2013). There are also other extrinsic toughening mechanisms which are discussed later in this chapter.

2.1 Biomimicry and Superhard Materials

Biomimicry is increasingly becoming a popular phenomenon in the design of novel material structures with an excellent combination of strength, hardness and toughness. The complex hierarchical microarchitectures of biological materials have already inspired the design of exceptionally tough ceramic composites (Chen et al. 2012; Karambelasa et al. 2013; Munch et al. 2008; Ritchie 2011; Sowmya et al. 2013; Torres-Sanchez and Corney 2011; Wang et al. 2000). These biomimicked multilayered composites exhibit levels of damage tolerance far greater than what can be achieved in monolithic structures. For example, Wang et al. (2000) produced fibrous and laminated silicon nitride—boron nitride (Si_3N_4/BN) composites imitating bamboos and nacre structures, respectively. In both cases, the materials showed over a tenfold increase in the work of fracture compared to monolithic silicon nitride (Si_3N_4) ceramics. Similar results were reported by Karambellas et al. (2013). They used a SHELL (sequential hierarchical engineered layer lamination) technique to fabricate Si_3N_4/BN ceramic composites mimicking the microarchitecture of *Strombus gigas* shell. Damage tolerance values of 8–9 times higher than that of monolithic Si_3N_4 were reported. These are only a few of several other examples where biomimetic ceramics and composites with

significantly higher fracture toughness compared to those of their constituents have been reported in literature (Chen et al. 2012; Munch et al. 2008; Ritchie 2011; Sowmya et al. 2013; Torres-Sanchez and Corney 2011). Understanding the functions of the microarchitectures of biomaterials with the view of replicating them in their synthetic counterparts forms a significant part of these studies.

Researchers have used several natural materials to inspire the design and fabrication of superior industrial materials. Examples of commonly used materials include bamboo, tooth, nacre, collagen fibres and bone. The bamboo is a functionally graded material with a hierarchical or layered structural design. The nodes, which occur periodically along the length of the bamboo, impart tensile strength, stiffness and rigidity on the macroscale (Amada 1995; Amada et al. 1997; Li et al. 2007). The microstructure changes gradually from outer to the inside of the material. Density of distribution of the vascular bundles, which act as the reinforcing component, is highest in the outer green layer, which experiences the maximum stresses during bending. Such a hierarchically designed structure is typical of biomaterials where an optimised structural design is used to realise superior mechanical performance. The bamboo also exhibits an asymmetric flexural and tension/compression behaviour when subjected to different loading states. Habibi et al. (2015) used multi-scale mechanical characterisations and microstructure analysis to investigate this behaviour in natural bamboo (*Phyllostachys edulis*) strips under different loading configurations (Habibi et al. 2015). They were able to show that the flexural asymmetry is mainly due to the gradient distribution of the vascular bundles along the thickness direction, whereas the hierarchical fibre/parenchyma cellular structure plays a critical role in alternating the dominant factors for determining the distinctly different failure mechanisms. A numerical model was also employed to study the effective flexural moduli of bamboo strips as a function of microstructural parameters. One of the peculiar aspects of the bamboo is the evolution of the microstructure of its outer and innermost layers under different bending states. This is important in distribution and transmission of stresses and also in relieving any local high stresses.

Other materials such as mammalian tooth (Sarikaya 2002), collagen fibres (Jager and Fratzl 2000) and bones (Buskirk et al. 2002) have also been studied and used. A mammalian tooth is an intricately structured and functionally graded composite, containing both the enamel (outer layer) and the dentin (on the inside) that are coupled through an interface region called dentin-enamel junction. The enamel is composed of long crystallites packed as bundles in enamel rods, which are organised unidirectionally normal to the tooth surface. This results in high hardness and wear resistance. The dentin is primarily composed of mineralised collagen fibres that form a randomly intertwined, continuous network. The result is a soft but highly tough material. Combining the two components (enamel and dentin) gives a functionally graded composite material with an excellent combination of hardness (on the contact surface), strength and good fracture toughness (provided by the tougher inner region). Figure 7.1a shows the schematic of a mammalian tooth. The ratio between the thickness of the enamel (d) and that of the dentin (R-d) is critical to realising the desired combination of hardness, strength and toughness. As shown

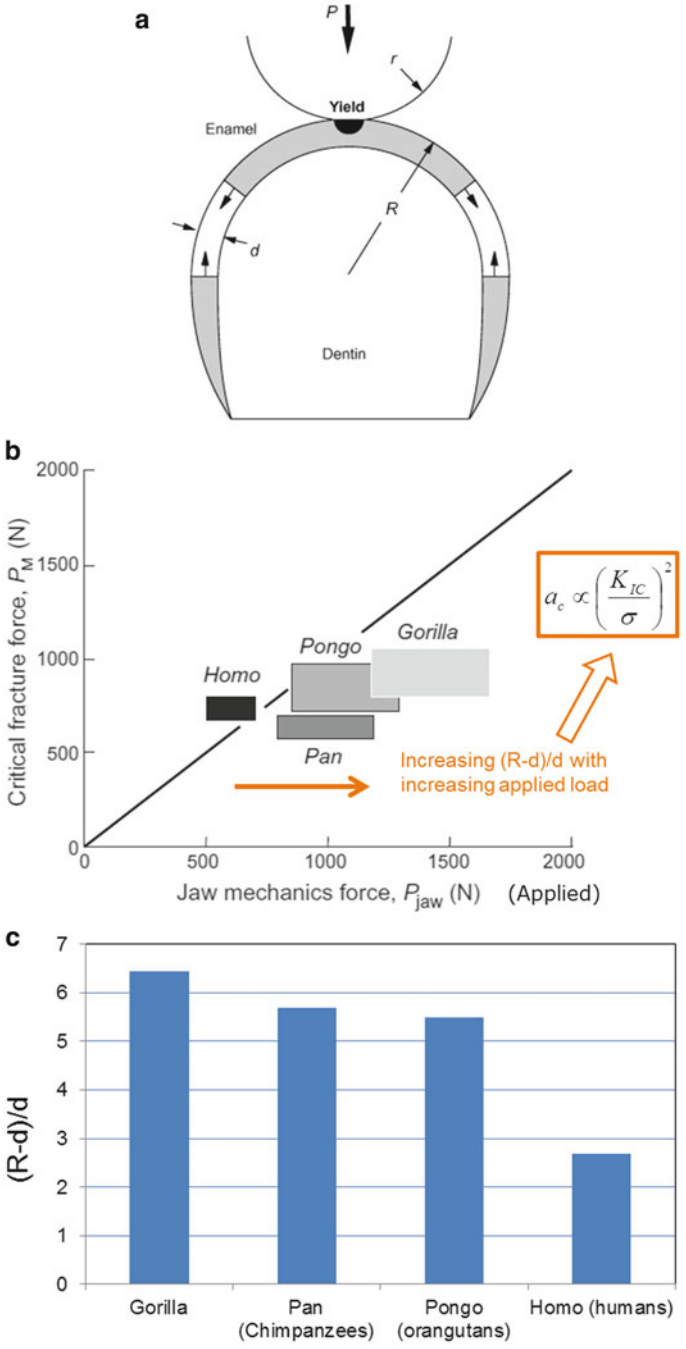

Fig. 7.1 (**a**) The schematic of a mammalian tooth structure showing the two regions, enamel and dentin, (**b**) and (**c**) the relationship between the force generated by jaw mechanics, critical fracture force and structure of the tooth in terms of the thickness ratio of the enamel to dentin (figures reproduced from data published by Lee et al. (2010))

by Lee et al. (2010), there is a correlation between this ratio and the allowable applied force. The integrated jaw mechanics design ensures that the maximum force that can be generated by the jaws does not exceed the tooth fracture load, thereby providing some safety measure.

The critical fracture force is the force required to induce cracks in the structure. Given that the microstructure composition of the enamel is similar between the different tooth types, this is fairly constant. However, different tooth structures allow for different crack lengths before catastrophic failure would occur. From Fig. 7.1b, c, it can be seen that as the applied load increases (i.e. jaw mechanics force), so does the (R-d)/d ratio. In other words, where higher loads are expected, the thickness of the enamel is desired to be a lot smaller than that of the dentin, i.e. a higher (R-d)/d ratio. This can be related to the critical flaw size concept as proposed in Griffith's failure criteria as given by Eq. 7.1:

$$a_c \propto \left(\frac{K_{IC}}{\sigma}\right)^2, \tag{7.1}$$

where a_c is the critical flaw size at which catastrophic failure occurs and K_{IC} and σ are, respectively, the mode I fracture toughness (critical stress intensity factor) and remotely applied load. This simply states that under given loading conditions, there exists a critical crack length at which catastrophic failure or fracture would occur. Assuming a constant value of K_{IC}, the critical flaw size varies inversely with the applied load. In the case of the tooth structure and the results of the study by Lee et al. (2010), it can be deduced that the ratio of the enamel thickness to that of the dentin, i.e. d/(R−d), behaves in a very similar way to the critical flaw size of Eq. 7.1.

The stiffness and toughness of this composite structure can also be easily estimated by using the analogue of springs in series. Take the example of two concentric layers in Fig. 7.2, composed of one inner region (material 1) with elastic modulus E_1 and thickness t_1 and outer region (material 2) with modulus E_2 and thickness t_1. The respective stiffness of the two regions, k_1 and k_2, can be determined as

$$k_1 = \frac{E_1 A}{t_1} \text{ and } k_2 = \frac{E_2 A}{t_2}, \tag{7.2}$$

where A is the unit cross-section area. The equivalent stiffness for springs connected in series is then given by

$$k_{eq} = \frac{1}{\frac{1}{k_1} + \frac{1}{k_2}} = \frac{1}{\frac{t_1}{E_1 A} + \frac{t_2}{E_2 A}} = \frac{E_1 E_2 A}{t_1 E_2 + t_2 E_1} \tag{7.3}$$

The equivalent elastic modulus, E_{eq}, is related to the equivalent stiffness through

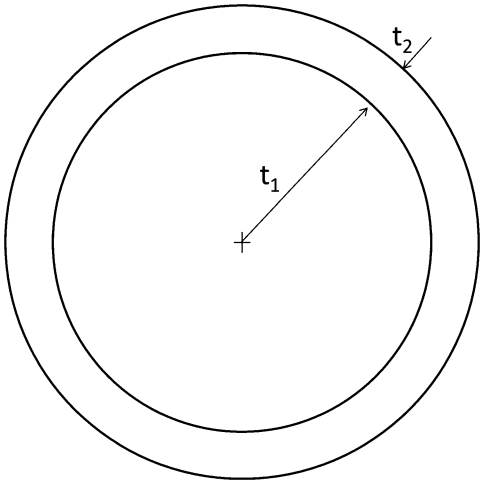

Fig. 7.2 Bi-concentric layered (functionally graded) structure

$$k_{eq} = \frac{E_{eq}A}{t_1 + t_2}, \text{ thus } E_{eq} = \frac{E_1 E_2 (t_1 + t_2)}{t_1 E_2 + t_2 E_1} \tag{7.4}$$

As the thickness of the outer layer, t_2, decreases, the stiffness of the composite approaches that of the inner region and vice versa. Similarly, the equivalent fracture energy values of a multilayered structure with layers arranged perpendicular to the direction of crack propagation can be treated as an additive quantity of respective volume ratios as shown in Eq. 7.5:

$$G_{eq} = \frac{G_1 t_1}{t_1 + t_2} + \frac{G_2 t_2}{t_1 + t_2}, \text{ and } G_{IC} = \frac{{K_{IC}}^2}{E} \text{ for a perfectly brittle material,} \tag{7.5}$$

where G_{IC} and K_{IC} are the mode I fracture energy and fracture toughness, respectively.

The structure of the bone is in many aspects different from the tooth and other natural materials as it is based on controlled porosity and density at several length scales. The observation that bones never fracture in the vicinity of the natural holes in them (where blood vessels pass through) is explained by the fact that the composition of the bone varies around the holes such that it is denser and stronger wherever the stresses are higher (in the vicinity of the hole) and less dense where it needs to be more flexible (weight-optimised solution). This again points to how intelligently biomaterials are designed (i.e. with a very high level of material efficiency and economy). These structures are also made of basic and relatively inferior materials such as calcium carbonate. However, the structures are highly optimised in order to realise properties and performance that is several orders of magnitude better than their constituents.

Collagen fibres are another natural material that can inspire the design of high-strength structural components. These fibres are composed of assemblies of parallel

collagen molecules arranged with a longitudinal stagger. It is thought that this staggered structure ensures much higher strength than can be realised from strictly parallel arrangement of collagen molecules or platelets (Jager and Fratzl 2000).

In terms of a natural material that has received a lot of attention over the years for its extraordinary mechanical performance and damage tolerance, and also mostly mimicked in material design, the nacre (abalone shell) tops the list. It is known to exhibit fracture toughness values that are 2–3 orders of magnitude higher than either of its constituent phases (Karambelasa et al. 2013; Ritchie 2011; Wang et al. 2000; Shao et al. 2013). This is usually attributed to its carefully arranged hierarchical multiphase, multilayered and functionalised brick-and-mortar architecture. The bricks or platelets, which are mineralised aragonite (calcium carbonate), form 95 vol.% of the structure separated by a protein layer (mortar) which forms the other 5 vol.% (Rabiei et al. 2010; Ritchie 2011; Shao et al. 2013). Despite this composition, it presents fracture toughness in energy terms of up to 3000 times higher than that of $CaCo_3$ (Wang et al. 2000). The platelets are closed-packed at a given layer, but they are staggered through the thickness. This hierarchic design results in a very high-performing material which easily adapts to different loading conditions. For example, when the resolved stresses are normal to the platelet plane, the organic matrix bridge between the platelets keeps them together and prevents uncontrolled crack growth. If the resolved stresses are shear, then the platelets slide successively over the organic matrix. This segmented layered structural design concept (used in nacre) can be used to design strong and yet tough materials for use in industrial applications such as superhard cutting tools.

The structure exhibits several levels of hierarchy, spanning all the way from nanoscale (e.g. mineral nanofibres and platelets imbedded within proteins) to micro- and macro-scales (Bechtle et al. 2010). Fundamentally, the nacre can be thought of as a brick-and-mortar structure as shown in Fig. 7.3.

The mineralised aragonite and organic biopolymer form the bricks and mortar, respectively. The bricks are approximately 0.5 um thick and 5–10 um wide (Ritchie 2011). The thickness of the organic layer (‘mortar’) is nanosize in dimensions with values of 10–45 nm reported in literature (Barthelat 2007, 2010; Barthelat et al. 2006; Lin and Meyers 2005; Nassif et al. 2005; Song and Bai 2003). The fracture-toughening mechanisms in the nacre can be assumed to occur at different length scales and both intrinsic and extrinsic. Intrinsic mechanisms refer to processes acting within the process zone ahead of the crack tip. These primarily relate to plasticity and are associated with making cracking or de-bonding more difficult by enlarging the plastic zone (Ritchie 2011). On the other hand, extrinsic toughening mechanisms relate to processes acting during crack propagation at the location of the crack to inhabit crack growth. These include formation of microcracks around the crack tip to reduce stress concentration, and crack bridging and friction interlocking in the wake of crack to induce some sort of crack closure (Ritchie 2011). Extrinsic toughening mechanisms arising from crack blunting, deflection and bridging at the brick-mortar interfaces have been suggested as the dominant factors in the high toughness of the nacre (Lin and Meyers 2005; Rabiei et al. 2010; Ritchie 2011). Crack deflections promote a more torturous crack path which

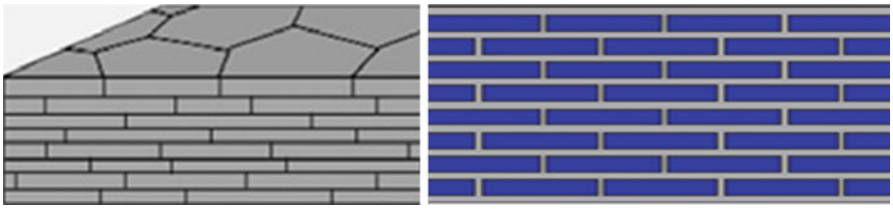

Fig. 7.3 A schematic representation of the nacre's microarchitecture (i.e. brick-mortar structure)

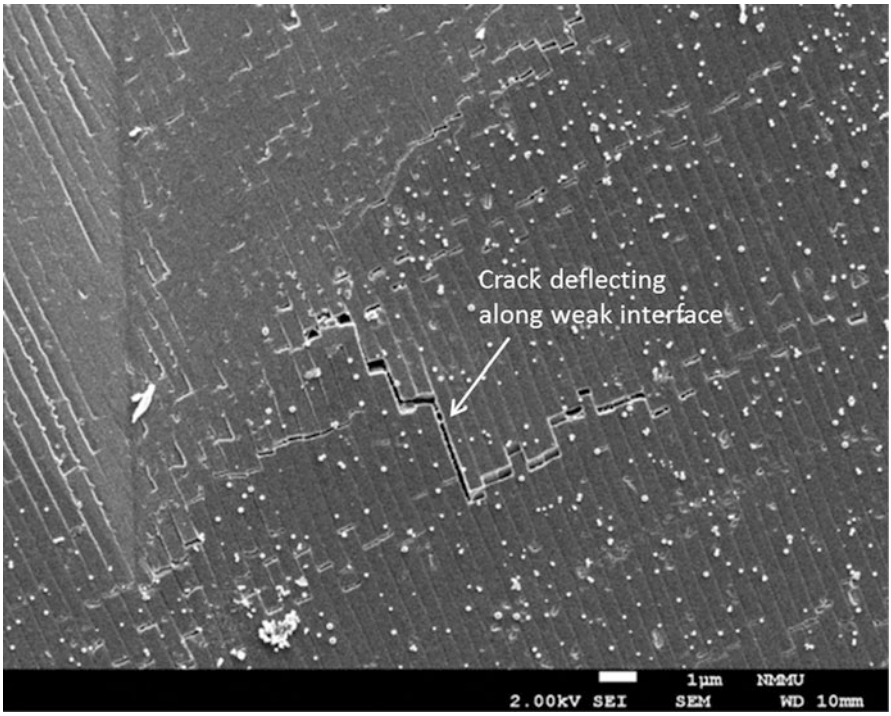

Fig. 7.4 Crack deflection in shell (nacre) structure subjected to indentation loading (in order to generate and propagate cracks in the structure). The work was performed by Dr. L. Westraadt (Nelson Mandela Metropolitan University, South Africa) on behalf of Element Six Ltd, UK

increases the resistance to crack growth. Figure 7.4 shows an example of crack deflection in a shell structure subjected to indentation loads in order to induce and grow cracks. The aim was to study the crack growth behaviour through the structure.

The pull-out effect of platelets acts as bridging elements and promotes transfer of stresses between crack surfaces (Lin and Meyers 2005; Rabiei et al. 2010). During relative sliding between neighbouring platelets, the organic ligaments are also thought to provide some bridging effect and transfer stresses (Barthelat and

Espinosa 2007; Shao et al. 2012). The adhesion between the platelets and the organic layer is very critical to the toughness of the nacre (Ritchie 2011). If the neighbouring platelets were strongly bonded together, the resulting toughness would be very low and close to that of a monolithic structure. A weak adhesion and lubricating effect provided by the organic layer allows for limited movement between the platelets. This helps relieve high local stresses and enhance the fracture toughness of the structure. However, excessive sliding between the platelets would render the material weak (Ritchie 2011). It is hypothesised that the roughened surfaces of the mineral platelets provide frictional stops which limit the amount of sliding (Chaia and Lawn 2004; Karambelasa et al. 2013; Ritchie 2011). In addition, small mineral 'bridges' linking the layers also help control the relative movement of the platelets.

Research has also shown that the fracture toughness of nacre exhibit a distinct dependence on the sizes and aspect ratios of platelets (Shao et al. 2012). This is important if the main toughening mechanism is due to crack bridging of platelets and their pull-out during the fracture process as suggested by several studies. Shao et al. (2012) showed that in order to achieve high toughness, the thickness of the platelets has to be in a certain range, with values of less than one micron proposed. On the other hand, very thin platelets are likely to break before being pulled out due to the tensile traction (Shao et al. 2012). A large aspect ratio was also suggested as beneficial for the improvement of toughness by crack bridging effect. However, it is extremely difficult to reproduce submicron features found in the nacre in most structural ceramics, and even more challenging in superhard materials, where the particle size of the powders used is already greater than a micron. In addition, having the necessary technology to replicate these structures or features at the same micro- and nanoscales is also a challenging task. Therefore, there is need to establish the most important design parameters for biomimicked ceramics between the size of the features, their aspect ratios, interface properties and stacking pattern. Effect of the interaction between these parameters is also of paramount importance.

Engineering weak interfaces in materials, either at the microstructure level or mesoscale, can greatly enhance the damage tolerance and resistance to fracture. The idea is to promote crack deflection along interface boundaries rather than cracks propagation through these boundaries. Two possible scenarios exist for a crack approaching an interface of two materials, i.e. deflect along the interface or penetrate through it. According to He and Hutchinson (1989), this is governed by the ratio between the energy required for crack deflection along the interface (G_d) versus that required for a crack to penetrate through the interface (G_p), given by Eq. 7.6:

$$\frac{G_d}{G_p} = \left(\frac{1-\beta^2}{1-\alpha}\right)\frac{|d|^2 + |e|^2 + 2\mathrm{Re}(de)}{c^2} \tag{7.6}$$

where α and β are Dundurs' parameters defined in He and Hutchinson (He and Hutchinson 1989) and c, d and e are complex valued functions of α and β. They

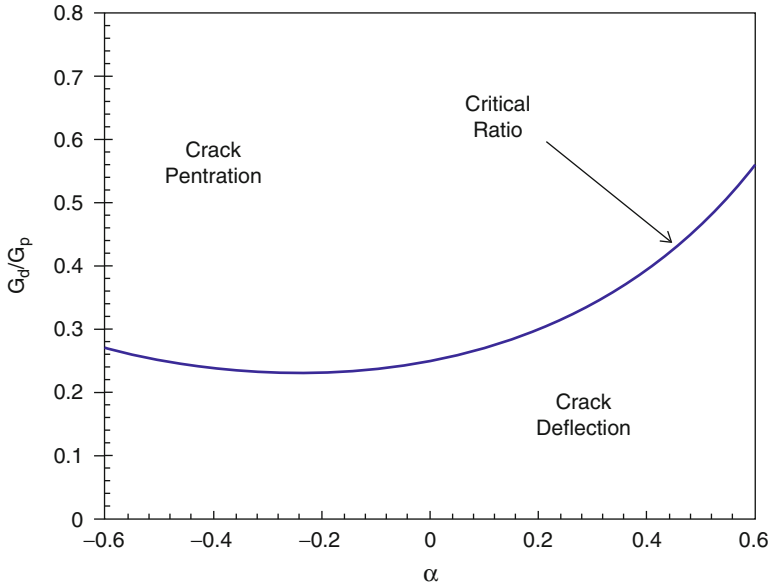

Fig. 7.5 Critical ratio of interface strength versus bulk material strength for crack deflection versus crack penetration as a function of α (data reproduced from He and Hutchinson (He and Hutchinson 1989), for α not too different to zero, the critical ratio is approximately 0.25. This corresponds to a case where the elastic properties are the same either side of an interface. The critical ratio increases to approximately 0.38 when $\alpha = 0.33$, corresponding to a modulus factor difference of two across a material interface)

reported that under given conditions, a critical ratio (G_d/G_p) exists below which crack deflection along the interface is favoured over crack penetration as illustrated in Fig. 7.5 (for $\beta = 0$). This is also confirmed in separate studies looking at crack propagation through multilayered structures (Carolan et al. 2013b). G_d and G_p can also be related to the maximum cohesive strength of the interface $\sigma_{\max}^{\text{int}}$ and the bulk $\sigma_{\max}^{\text{bulk}}$, respectively, via cohesive zone model (CZM). Therefore a critical ratio between $\sigma_{\max}^{\text{int}}$ and $\sigma_{\max}^{bulk}$ can also be determined below which crack deflection would be preferred over penetration.

Understanding this relationship between G_d and G_p is important if one wants to exploit this crack deflection mechanism in order to develop tough and damage-tolerant material. This toughening mechanism is also one of the most important in the nacre (Fig. 7.4). If the layers or 'bricks' are strongly bonded, crack penetration through the interface is more likely to occur than crack deflection. Similar results to Fig. 7.4 can also be obtained via a numerical analysis of crack growth through a brick-mortar structure mimicking the nacre. A single-edge notched sample is loaded in a three-point bend test set-up as shown in Fig. 7.6. The sample size is 36 um long and 8 um wide, with a pre-crack length $a = 2$ um and span $S = 32$ um.

The interface properties are chosen such that crack deflecting and propagation along the interface is preferred over crack penetration through the interface. This is

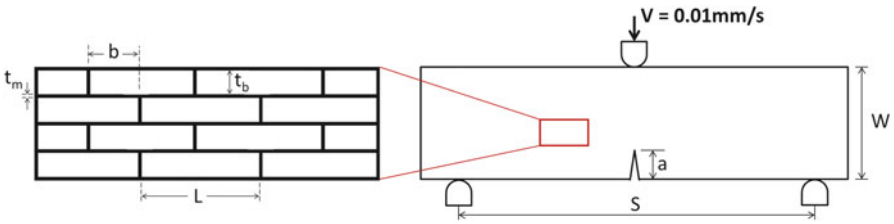

Fig. 7.6 Geometry for numerical modelling of crack propagation through a brick-mortar structure, mimicking the nacre

determined using the analysis proposed by He and Hutchinson (1989) as discussed earlier. The optimum value of σ_{max}^{int} was found to be one third of σ_{max}^{bulk}. With this value, crack propagation is predominantly through the interface (mortar). However, this also depends on other factors such as the thickness of the bricks (t_b), aspect ratio (L/t_b) and stacking pattern. The properties of the platelets used are approximated based on reported literature values for aragonite calcium carbonate, i.e. Young's modulus E = 70 GPa, cohesive strength $\sigma_{max}^{bulk} = 100$ MPa, fracture energy G = 0.1 J/m^2, density rho = 2830 kg/m^3 and Poisson's ratio = 0.1 (Bechtle et al. 2010). Details of the numerical procedure can be found in Appendix 7.1.

It is shown in these results that the work of fracture is significantly higher when cracks are forced to deflect along weak interface boundaries rather than propagating through them (Fig. 7.7).

Structures such as the nacre can be used to inform the design of superhard materials with greatly enhanced toughness. Such materials would truly revolutionise the superhard material market, especially in cutting/machining and drilling applications. They would offer high reliability, durability and predictable cutting tool breakdown characteristics. These aspects are currently lacking in traditional superhard and ultrahard materials such as polycrystalline cubic boron nitride and diamond.

2.2 *Other Ways of Creating Exceptionally Tough Superhard Materials*

Apart from mimicking natural materials, there are also other general methods of designing superhard materials with superior toughness. Examples of these include dispersing a tough phase in a superhard material matrix (Khan et al. 2010; Li et al. 2008a; Oksman and Craig 1998; Roether and Baccaccin 2005; Yun et al. 2004), engineering controlled defects (Evans et al. 1997; Hutchinson 1989; Shum and Hutchinson 1990), functionally graded structures (Buskirk et al. 2000; Baccaccini 2005; Jeong-Ho and Paulino 2002; Mishnaevsky 2005; Munch et al. 2008), nanostructuring (Li et al. 2008a, b; Tan and Wie 1998), imbedding a three-dimensionally interpenetrating network of a tough phase inside a brittle

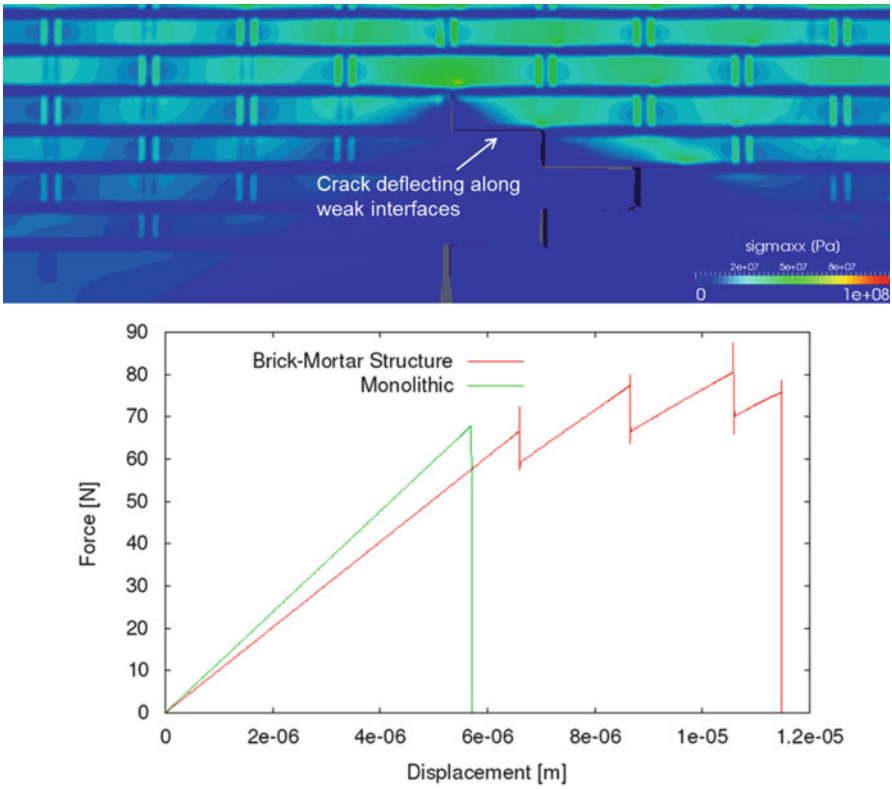

Fig. 7.7 Numerical prediction of crack growth through the brick-mortar structure, showing crack deflection along weak interfaces (*top*). The work of fracture is significantly higher in a brick-mortar structure compared to a monolithic one (*bottom*). This is mainly due to the structure providing a more torturous path for crack. Bricks with high aspect ratios may also provide an interlocking mechanism and contribute to the increasing R-curve behaviour

matrix (Lin et al. 2014; Wang et al. 2010; Wanga and Liu 2008) and several other toughening mechanisms extensively covered in literature. The above mechanisms are also key features of natural materials as seen in the previous section (i.e. Sect. 2.1). The general concept of functionally graded structures, apart from it being a key aspect of biomimicked materials, has been extensively used in order to design engineering materials with a good combination of toughness and hardness (or strength). Functionally graded materials are composites in which the volume fraction of constituent materials varies gradually, usually along the component's thickness. The result is a non-uniform microstructure with continuously graded macro-properties. The 'layers' are stacked in a predefined sequence in order to achieve desired properties, which are usually superior in comparison to monolithic materials (Mishnaevsky 2005; Munch et al. 2008). Such designs open up several opportunities for optimising both material and component structures to achieve high performance and material efficiency (Jeong-Ho and Paulino 2002) and can be

adapted to most industrial materials (including the superhard materials) design relatively easy.

The technique of using layered structures or functionally graded materials is now widely being used in designing ceramics with enhanced fracture toughness (Buskirk et al. 2002; Jeong-Ho and Paulino 2002; Mortensen and Suresh 1997). In many ways and as seen in Sect. 2.1, these designs are inspired by biomaterials whose extraordinary properties are thought to result from their peculiar microstructures, i.e. architecture and arrangement and distribution of the microstructural elements. The emphasis in these functionally graded materials is to achieve an optimum combination of two or more properties, e.g. hardness and toughness. For example, Fig. 7.8 shows the results of numerical modelling of crack propagation through a graded structure consisting of a relatively tougher material ('blue', material A) sandwiched between layers of a less tough one ('red', material B). The properties of material A (red) and material B (blue) are summarised in Table 7.1. The numerical model employs a cohesive zone model (CZM) approach with crack growth taking place through the natural process of de-bonding of the cohesive zone under loading (Carolan et al. 2013b). Details of the numerical procedure can be found in Appendix 7.1.

It is clear that a graded structure offers more resistance to crack growth as indicated by the time taken for crack to grow by a similar length under identical loading conditions compared to a monolithic structure (which is composed of only material B). In the monolithic structure, it takes the crack 10 microseconds to grow by 7.5 mm, whereas the time required in a graded structure is 160 microseconds, representing a 16-fold increase.

A superhard material can also be toughened by dispersing a second phase in its matrix. This toughening mechanism has already been successfully employed to improve fracture toughness in brittle ceramics. The process normally involves adding a tougher dispersed phase to a ceramic matrix. Examples include the works of Walter et al. (1997), Magniez et al. (2011), Evans (1997), Raj and Thompson (1994) and Tan and Wie (1998). A tougher second phase network would absorb energy through plastic deformation and hence retard crack growth or extension. On the other hand, it was also shown by Evans (1997) and Evans et al. (1997) that the second dispersed phase does not necessary has to be a ductile phase. It can be brittle second phase particles which fail in the stress field of a growing crack, resulting in controlled microfracture. The goodness with using brittle particles is that the overall hardness of the composite would not be sacrificed but may even be further enhanced. This would open up possibilities of designing superhard materials (i.e. diamond and cubic boron nitride composites) with favourable fracture performance without any deterioration in abrasion resistance. The dispersed second phase can also be used as localised stress raisers which would facilitate crack bifurcation and/or multiple crack fronts, resulting in increased fracture resistance. The concept of toughening by microcracks has been suggested by a number of researchers (Evans et al. 1997; Hutchinson 1989; Shum and Hutchinson 1990). The rationale is to minimise the maximum energy release rate (G) among the various crack tips. Therefore, a material that can generate multiple

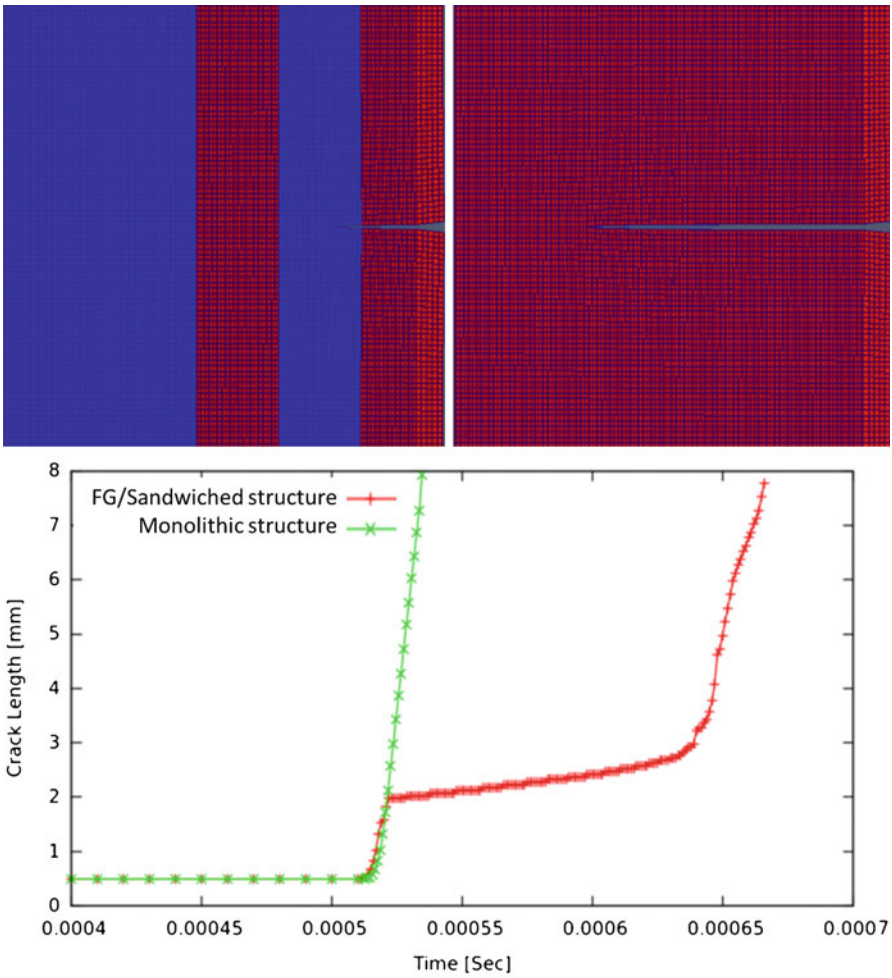

Fig. 7.8 Numerical simulation of crack propagation through a graded structure consisting of a relatively tougher material ('*blue*', material A) sandwiched between layers of a less tough one ('*red*', material B) as shown in top images. The graded structure offers better resistance to crack propagation that a monolithic one

Table 7.1 Material properties of material A and material B, with the former being the tougher of the two materials

Material property	Material A	Material B
E	900 MPa	1000 MPa
G	81 J/m^2	40 J/m^2
σ_{max}	1200 MPa	1600 MPa

cracks under loading would behave tougher than a material with only one major crack since multiple crack fronts entail that the net energy supplied to a system has to be divided up between several cracks, resulting in a much slower rate of crack growth. The other mechanism that can be facilitated by inducing evenly or randomly distributed/dispersed micro-defects in a material is that it would facilitate crack bifurcation. The size, shape and distribution of these micro-defects are critical and would, thus, require to be optimised. Based on this optimisation, it is possible to improve fracture resistance without significantly compromising the overall strength and hardness of the material, which is desirable for superhard materials.

In order to fully realise the benefit of using a 'second dispersed phase' as a toughening mechanism, one has to consider several key factors that require optimisation. These include the volume fraction of the dispersed phase; the microstructural parameters of the inclusions such as shape, aspect ratio and size; and the differences in elastic properties, strength and fracture toughness of the matrix and inclusions. In addition, the thermal expansion mismatch between the matrix and inclusions need to be optimised in order to get a favourable residual stress state of the resulting composite/structure. The properties of the matrix/inclusion interfaces are also important, i.e. whether one requires that the inclusions are strongly or weakly bonded to the matrix. The latter may be beneficial in deflecting cracks at the interfaces between the inclusions and the matrix as discussed earlier in the case of the nacre (Sect. 2.1).

Apart from the toughening mechanisms discussed above, there are still several others that can potentially be applied to superhard materials. The most important aspect is controlling what is happening in the vicinity of a growing crack (controlled microfracture) such as through transformation toughening and crack shielding (Ritchie 1999). However, to be able to appreciate these mechanisms and effectively employ them to improve a material's fracture resistance, one has to first understand the mechanisms of crack propagation in superhard materials, which by their nature are intrinsically brittle. The mechanisms of crack growth in brittle materials are quite distinct from those commonly encountered in ductile materials such as metals. In the later, crack growth is predominantly due to intrinsic microstructural damage mechanisms, which promote crack extension ahead of the crack tip, whereas in brittle materials it is usually controlled by extrinsic crack-tip shielding mechanisms which act primarily behind the crack tip to retard crack growth (Ritchie 1988, 1999). Figure 7.9 illustrates the two competing toughening mechanisms, i.e. extrinsic toughening which is predominant in brittle materials and intrinsic toughening which dominate fracture in ductile materials.

In ductile materials, intrinsic damage mechanisms typically involve processes which create microcracks or voids, e.g. by dislocation pile-ups or interface decohesion, in the highly stressed region ahead of the crack tip, leading to classical failure by cleavage, intergranular cracking or microvoid coalescence, and may also involve the repetitive blunting and resharpening of the crack tip in the case of cyclic loading (Neumann 1969). The creation of several microcracks in a highly stressed region, which precedes microcrack coalescence, is one of the main reasons for the high toughness of ductile materials. Extrinsic shielding mechanisms are caused by the creation of inelastic zones in the crack wake or from physical contact between

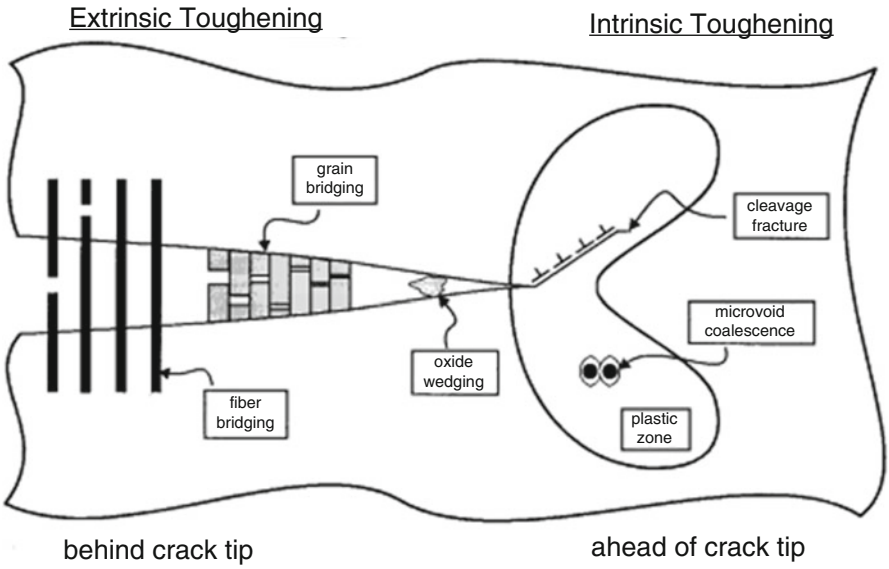

Fig. 7.9 Competition between extrinsic and intrinsic toughening mechanisms, with the former controlling the fracture process in brittle materials (Ritchie 1999)

the crack surfaces via wedging, bridging, sliding or combinations of these factors (Ritchie 1988). The typical example is 'zone shielding' such as transformation and microcrack toughening in ceramics and rocks, where the in situ dilatant phase transformations or the microcracking of precipitates/particles ahead of the crack tip can lead to inelastic zones in the crack wake which impart closing tractions on the crack surfaces (Ritchie 1988). The other example is that of 'contact shielding' caused by bridging tractions imposed across a crack by unbroken fibres, laminated layers or a particulate phase in composite materials, or the wedging of corrosion debris or fracture surface asperities during crack closure. Its should be noted here that intrinsic mechanisms are an inherent property of the material and thus are active irrespective of the length of the crack or the geometry of the test specimen and control the driving forces (e.g. the stress intensity or mode I, II and III fracture toughness) responsible for initiating a crack. On the other hand, extrinsic mechanisms act in the crack wake and, hence, are critically dependent on crack size and responsible for the development of resistance-curve (R-curve) behaviour resulting in improved fracture resistance (e.g. Evans 1997; Becher 1991). For example, Evans (1997) demonstrated that more than a fivefold increase in fracture toughness of zirconia can be achieved by inducing an in situ phase transformation at the crack tip (transformation toughening) or by causing the in situ microcracking of particles (microcrack toughening), both processes causing a dilation around the crack tip which is constrained by surrounding elastic material. There are several literatures that the reader can consult on toughening mechanisms and how they can be applied to inherently brittle materials such as the superhard materials discussed in this chapter.

3 Cost-Effective Manufacturing and Processing of Superhard Materials

The manufacturing and processing of traditional superhard materials, e.g. diamond and cubic boron nitride, is extremely challenging and expensive. In order to synthesis these materials, one requires access to extremely high temperatures and pressures usually in excess of 1400 °C and 5 GPa, respectively. In addition, processing superhard materials into final formats required by end users using traditional material removal machining methods is not a trivial task. All these have an impact on the overall cost of manufacturing superhard materials for cutting tools. The other challenge is that industry continues to require superhard parts and cutting tools with complex geometries. Unfortunately, traditional superhard material manufacturing technologies lack the ability to compete in a market where customers require customised complex components. This challenge can be overcome by additive manufacturing, in particular 3D printing, given the nearly unlimited design freedom that it provides (Faes et al. 2015). In addition, using additive manufacturing technologies would not only reduce material waste but also a significant step towards reducing the current costs associated with superhard materials manufacturing and processing.

3.1 Additive Manufacturing Technologies

As cutting tools and other superhard parts continue to require more intricate geometries such as chip-breakers, additive manufacturing technologies such as 3D printing or laser sintering will be key enablers to realising this at a favourable cost. Current methods of preparing such geometries are based on machining already sintered polycrystalline diamond or cubic boron nitride blanks/blocks either using laser ablation, electron discharge machining or via mechanical grinding operation. The ability to form the required final geometry via additive manufacturing is an appealing concept. However, the biggest challenge is that the sintering or synthesis of both diamond and cubic boron nitride needs high pressure due to their phase transformations at higher temperatures required to form sintered bodies (see Chap. 2 for details). Therefore, the most feasible approach at the moment is forming near net-shaped green bodies of required geometries via appropriate techniques such as 3D printing and then subjecting such geometries to the high pressure and high temperature sintering process. This does not necessarily reduce the high cost of the HPHT process but having a near net-shaped part reduces the amount of further processing required. The other thing that 3D printing techniques offer is the ability to form very intricate shapes which cannot be achieved any other way in a cost-effective manner. The current printing technologies can now produce parts to the resolution of few microns.

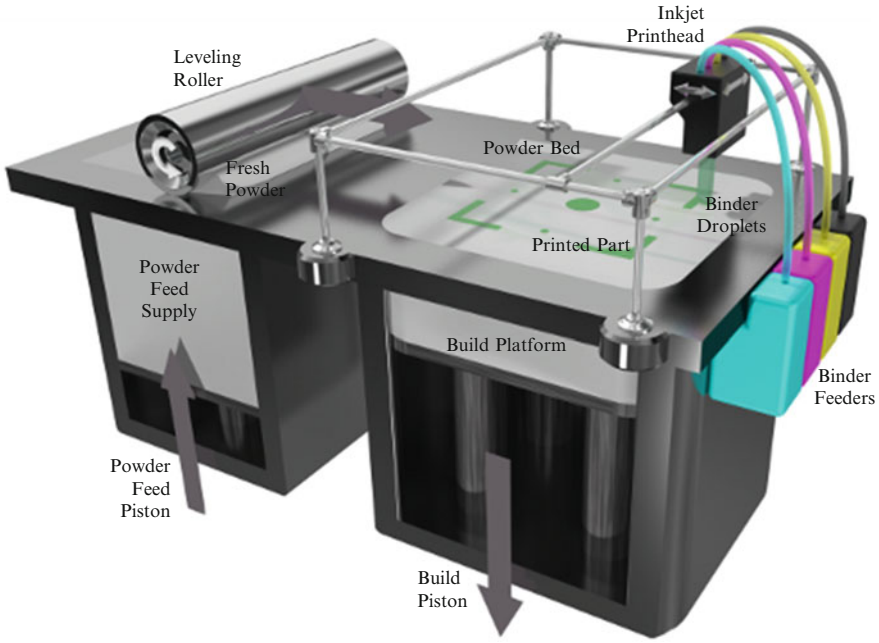

Fig. 7.10 Schematic of the Inkjet 3D printer from http://techrefectory.blogspot.co.uk (author: Sahil Bansal)

Three-dimensional printing is a layer-type additive manufacturing technique involving the deposition of powdered material in layers and selective binding of the powder by either 'inkjet' printing of a binder material or laser sintering. The unbound powders are then removed in order to recover the printed part. This process can be applied to the production of metal, ceramic and metal/ceramic composite parts. Figure 7.10 shows the schematic of a typical inkjet 3D printer used for printing ceramic parts.

3D printing provides significant opportunities for additive manufacturing of hard metals and superhard products. Applications for such may include microwear parts in electronic applications, mechanical components, complex moulds and dies and specialist cutting tools with integral coolant channels (Brookes 2015). Other applications are for printing ceramic and superhard microinjection moulding dies and moulds for handling superabrasive materials. Several researchers are already using 3D printing to manufacture hard metal parts and coatings. Zhang et al. (2015) employed 3D printing, which in their study is referred to as 'Laser Engineered Net Shaping (LENS™)', to deposit hard coatings of Ti-Si-N with three different Ti-Si ratios on commercially pure titanium substrate (Zhang et al. 2015). The coatings were later analysed and found to show graded microstructures and in situ formed phases. The hardness of the coatings were found to be favourable but with still a lot of scope for optimisation. Nevertheless, the possibility to use 3D printing for this purpose was demonstrated. Other examples include the work of Fu et al. (2013)

who fabricated silicon/silicon carbide ceramic composites using 3D printing of Si/SiC/dextrin powder blends. In this case, the parts (green bodies) had to undergo further heat treatments before final parts were realised. Companies such as NanoSteel have been using 3D laser printing/sintering to manufacture high-hardness ferrous metal matrix composite (MMC) parts using nano-particulate powders (NanoSteel 2015). The parts are prepared in a single 3D printing step and do not need to undergo any further processing and are reported to be 99.9 % dense, crack-free and with the wear resistance matching M2 tool steels made via conventional subtractive manufacturing technology (i.e. casting and machining). The hardness of these printed parts is about 61.91 HRC (Hardness Rockwell C). The lack of post-processing is thought to be a significant benefit as it reduces production costs. Kennametal and Valenite corporations are also looking into the fabrication of cemented carbide (i.e. tungsten carbide/cobalt) cutting tools using 3D printing (http://www.mit.edu/~tdp/6.html). In this case, the key opportunity that additive manufacturing is thought to offer over the current practice of dry pressing is the several degrees of flexibility (including geometry, in composition and in response to market demand).

Three-dimensional printing can also be integrated with other manufacturing and processing technologies. For example, Ahn et al. (2015) developed a novel nano-scale 3D printing process that integrated nanoparticle printing, micromachining and focused ion beam technology. An aerodynamically focused nanoparticle (AFN) printing, which is a room-temperature direct printing technique using shock-induced aerosol generation, was adopted for material formation, and focused ion beam was used for profiling the positioned material. In order to assist and bridge these two processes at different scales, micromachining using tools with diameters of 30 μm was employed. This integrated process enabled various 2.5D and 3D structures to be printed using metal/ceramic nanoparticles with no requirement for any post-treatment (Ahn et al. 2015).

It is clear that the current market trend is pushing towards the use of these additive technologies in order to reduce material waste/cost, increase responsiveness to market needs (especially for customised and complicated 3D shapes) and eliminate the need for post-processing (i.e. towards a single-step manufacturing process). Superhard materials and products would greatly benefit from such technologies given the challenges they present during post-processing steps in order to make the final geometries required by end users. There is also an increasing market need for micro-tools with 3D complex geometries which probably would not be made any other way other than through 3D printing or similar technologies.

Appendix 7.1: Numerical Modelling of Crack Propagation

The numerical model employs a cohesive zone model (CZM) to simulate crack propagation, using OpenFOAM software (a 3D finite volume C++ library). Fatigue crack growth is also incorporated into the model through the introduction

of a damage variable, D, into the CZM. Damage accumulates until sufficiently high to initial a crack or extend an already existing one. Cracks are grown through the natural process of de-bonding of the cohesive zone under cyclic loading. Decaying cohesive properties means that energy dissipation under fatigue fracture is less than the material toughness under monotonic loading. The model had been validated separately using experimental data before being employed in this analysis.

Numerical Analysis

The Cauchy momentum balance equation for a continuous media, neglecting body forces and assuming infinitesimal displacements U, can be given by

$$\rho \frac{\partial^2 \mathbf{U}}{\partial t^2} = \nabla . \boldsymbol{\sigma}, \tag{7.7}$$

where ρ is the density and $\boldsymbol{\sigma}$ is the Cauchy stress tensor defined by the constitutive law. In the case of an isothermal multi-material linear elastic model, $\boldsymbol{\sigma}$ is given by

$$\boldsymbol{\sigma} = \mu \left[\nabla \mathbf{U} + (\nabla \mathbf{U})^{\mathrm{T}} \right] + \lambda \, \mathrm{tr}(\nabla \mathbf{U}) \mathbf{I}, \tag{7.8}$$

where μ and λ are the shear modulus and second lame coefficient, respectively, and ∇ is the gradient operator. The normal and tangential components of the traction vector $\mathbf{t} = \mathbf{n}.\boldsymbol{\sigma}$ can be expressed as shown by [ZT,Alojz] given in Eqs. 7.8 and 7.9:

$$t_n = (2\mu + \lambda) \, \mathbf{n}.\nabla \mathbf{U} - (\mu + \lambda) \, \mathbf{n}.\nabla \mathbf{U}_t + \lambda \, \mathbf{n} \, \mathrm{tr}(\nabla_t \mathbf{U}_t) \tag{7.9}$$

$$\mathbf{t}_t = \mu \, \mathbf{n}.\nabla \mathbf{U}_t - \mu \nabla_t U_n \tag{7.10}$$

where $\nabla_t = (\mathbf{I} - \mathbf{nn}).\nabla$ is the tangential gradient operator and $\mathbf{n}$ is the unit normal vector. The subscripts n and t represent the normal and tangential components of the vector, respectively. A cohesive zone model (CZM) is employed to predict the fracture process. This assumes the fracture formation as a gradual phenomenon in which the separation of the new crack surfaces takes place across an extended crack tip, or cohesive zone, and is resisted by cohesive tractions as shown in Fig. 7.11 (Carolan et al. 2013b). Crack growth is through the natural process of de-bonding of the cohesive zone under loading. The numerical procedure allows prediction of crack propagation along internal control volume faces. When the failure criterion is satisfied (i.e. $t_n \geq \sigma_{\max}$ mode I and $\mathbf{t}_t \geq \tau_{\max}$ for mode II), these internal faces are transformed into cohesive zone boundary faces. $\sigma_{\max}$ and $\tau_{\max}$ represent the maximum cohesive strength of the material in tension and shear, respectively. The traction forces specified at the new boundary faces follow a prescribed traction-separation law or cohesive zone model.

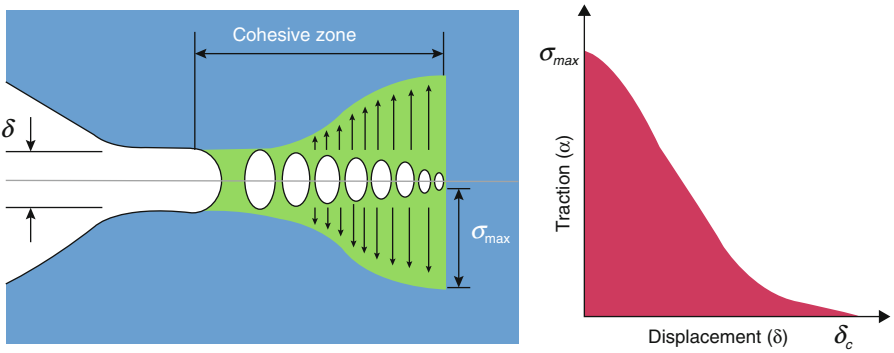

Fig. 7.11 Traction-separation relationship in the cohesive zone (Reproduced from (Carolan et al. 2013b))

The current study employs a linear cohesive zone model. This only requires two parameters to fully describe the model, i.e. the fracture energy G_c and the maximum cohesive strength as shown in Fig. 7.5 for mode I and mode II crack, respectively. Cracks can initiate and propagate under any of the two models, or a mixture thereof, depending on which condition is satisfied. According to the model, the traction between cohesive faces decreases with the separation distance between the faces. Fracture is assumed to have taken place when the critical separation distance is reached. At this point the cohesive faces become traction-free. Under all scenarios (i.e. mode I, mode II and mixed mode I & II), both the opening normal t_{cn} and shear t_{ct} cohesive tractions are assumed to decrease at the same rate.

For Mode I

$$t_{cn} = \sigma_{\max}\left(1 - \frac{\delta}{\delta_C}\right) \text{and} \, t_{cn} = \sigma_{\max}\left(1 - \frac{\delta}{\delta_C}\right) \tag{7.11}$$

For Mode II

$$t_{ct} = \tau_{\max}\left(1 - \frac{\gamma}{\gamma_C}\right) \text{and} \, t_{cn} = \sigma_{\max}\left(1 - \frac{\gamma}{\gamma_C}\right) \tag{7.12}$$

where δ and γ, are respectively, the normal and tangential components of the separation distance and the subscript C denotes the critical values at which cohesive

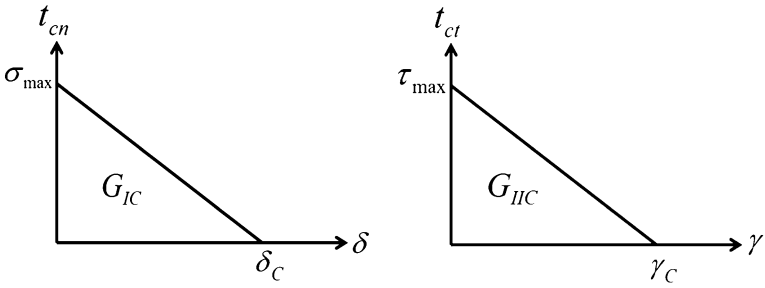

Fig. 7.12 Mode I (*left*) and Mode II (*right*) traction-separation laws, linear model

faces become traction-free. In the case of mixed mode I and II crack, the effective traction t_{eff}, effective separation distance δ_{eff} and effective maximum cohesive strength $\sigma_{\max}^{eff}$ are used instead:

$$t_{eff} = \sqrt{t_n^2 + |\mathbf{t}_t|^2} \geq \sigma_{\max}^{eff} \text{ and } \sigma_{\max}^{eff} = \sqrt{\sigma_{\max}^2 + \tau_{\max}^2} \tag{7.13}$$

$$\delta_{eff} = \sqrt{\delta^2 + \gamma^2} \text{ and } \sigma_{\max}^{eff} = \sqrt{\delta_C^2 + \delta_C^2} \tag{7.14}$$

The traction between the cohesive faces is then defined by

$$t_{cn} = t_{0n}\left(1 - \frac{\delta_{eff}}{(\delta_{eff})_C}\right) \tag{7.15}$$

$$t_{ct} = t_{0t}\left(1 - \frac{\delta_{eff}}{(\delta_{eff})_C}\right) \tag{7.16}$$

where t_{0n} and t_{0t} are the initiation tractions in the normal and tangential directions determined when the condition $t_{eff} = \sqrt{t_n^2 + |\mathbf{t}_t|^2} \geq \sigma_{\max}^{eff}$ is satisfied (Fig. 7.12).

Fatigue Crack Growth

For modelling fatigue crack growth, a damage variable, D, is introduced into the cohesive zone model (Abdul-Baqi et al. 2005; Arias et al. 2004; Roe and Siegmund 2003; Ural et al. 2009). A crack is initiated or extended when the combination of accumulated damage and traction satisfies the failure criteria, i.e. $t_n \geq \sigma_{\max}(1 - D)$

for mode I. The same applies to mode II and mixed mode. The damage accumulated during each time step (or loading cycle) ΔD is given by

$$\Delta D = (1 - D)^m \frac{\left|\Delta\widetilde{\delta}\right|}{\delta_C} \left[\frac{t - \sigma_{th}}{\sigma_{\max}}\right] \text{and} \, \Delta D \geq 0 \tag{7.17}$$

where m is a constant which control the decay of the reaction force at the final stage of damage (Abdul-Baqi et al. 2005), t is the traction at a face (normal traction in case of mode I fracture), $\Delta\widetilde{\delta}$ is the incremental deformation or loading separation distance and σ_{th} is the material's fatigue threshold (or fatigue endurance limit). The condition $\Delta D \geq 0$ ensures that the accumulated damage is always positive and either increases or stays the same with successive loading cycles. A zero value of m indicates that total accumulated damage, D, is not taken into account when calculating ΔD, and the opposite being true for a non-zero value. The total accumulated damage (during current time step or current loading cycle), D_{t_n} is, thus, given by

$$D_{t_n} = D_{t_{n-1}} + \Delta D \tag{7.18}$$

where $D_{t_{n-1}}$ is total damage during the previous time step. The following observations can be made from the above Eqs. 7.7 to 7.9.

- The crack only initiates or extends if damage, accumulated or current, is greater than some critical value. $D_{\max}$, for a given traction, t.
- The increment in damage is related to the increment in deformation, $\Delta\widetilde{\delta}$, weighted by the current traction or load level.
- There exists a fatigue limit, σ_{th}, below which cyclic loading can proceed infinitely without failure. Damage can only accumulate if the current traction is above this limit.

The modified cohesive parameters, taking into account the accumulated damage, can thus be defined as for mode I: $\widetilde{\sigma}_{\max} = \sigma_{\max}(1 - D_{\max})$ and $\delta_C = \delta_C(1 - D_{\max})$.

References

Abdul-Baqi A, Schreurs P, Geers M (2005) Fatigue damage modelling in solder interconnects using a cohesive zone approach. Int J Solids Struct 42:927–942

Ahn S-H, Yoon H-S, Jang K-H, Kim E-S, Lee H-T et al (2015) Nanoscale 3D printing process using aerodynamically focused nanoparticle (AFN) printing, micro-machining, and focused ion beam (FIB). CIRP Ann Manuf Technol 64(1):523–526, ISSN 0007–8506

Amada S (1995) Hierarchical functionally gradient structures of bamboo. Funct Gradient Mater 20 (1):35–37

Amada S, Ichikawa Y, Munekata T, Nagase Y, Shimizu H (1997) Fibre texture and mechanical graded structure of bamboo. Compos Part B: Eng 28(1–2):13–20
Arias I, Serebrinsky S, Ortiz M (2004) A cohesive model of fatigue of ferroelectric materials under electro-mechanical cyclic loading. Active Mater Behav Mech Proc SPIE, 371–377
Arsecularatne JA, Zhang LC, Montross C (2005) Wear and tool life of tungstene carbide, PCBN and PCD tools. Int J Mach Tools Manuf 46(5):482–491
Baccaccini A (2005) Glass-containing composite materials: alternative reinforcement concepts. In: Handbook of ceramic composites. Springer, Bostan
Barry J, Byrne G (2001) Cutting tool wear in the machining of hardened steels: Part II: cubic boron nitride cutting tool wear. Wear 247(2):152–160, ISSN 0043–1648
Barthelat F (2007) Biomimetics for next generation materials. Philos Trans R Soc A 365:2907–2919
Barthelat F (2010) Nacre from mollusc shells: a model for high-performance structural materials. Bioinsp Biomim 5:035001
Barthelat F, Espinosa HD (2007) An experimental investigation of deformation and fracture of nacre – mother of pearl. Exp Mech 47:311–324
Barthelat F, Li CM, Comi C, Espinosa HD (2006) Mechanical properties of nacre constituents and their impact on mechanical performance. J Mater Res 21:1977–1986
Barthelat F, Tang H, Zavattieri PD, Li CM, Espinosa HD (2007) On the mechanics of mother-of-pearl: a key feature in the material hierarchical structure. J Mech Phys Solids 55:306–337
Becher P (1991) Microstructural design of toughened ceramics. J Am Ceram Soc 74:255–269
Bechtle S, Fung Ang S, Schneider GA (2010) On the mechanical properties of hierarchically structured biological materials. Biomaterials 31:6378–6385
Brookes KJA (2015) 3D-printing style additive manufacturing for commercial hardmetals. Metal Powder Rep 70(3):137–140, ISSN 0026–0657
Buskirk SR, Venkataraman S, Ifiu PG, Rapoff AJ (2002) Functionally graded biomimetic plate with hole Collection of Technical Papers – AIAA/ASME/ASCE/AHS/ASC Structures. Struct Dyn and Mat Conf 2:1015–1021
Carolan D, Ivanković A, Murphy N (2013a) A combined experimental–numerical investigation of fracture of polycrystalline cubic boron nitride. Eng Fract Mech 99:101–117. doi:10.1016/j.engfracmech.2012.09.008, ISSN 0013–7944
Carolan D, Tuković Z, Murphy N, Ivanković A (2013b) Arbitrary crack propagation in multi-phase materials using the finite volume method. Comput Mater Sci 69:153–159, ISSN 0927–0256
Chaia H, Lawn BR (2004) Fracture mode transitions in brittle coatings on compliant substrates as a function of thickness. J Mater Res 19(6):1752–1761
Chen P-Y, McKittrick J, Meyers MA (2012) Biological materials: functional adaptations and bio-inspired designs. Prog Mater Sci 57:1492–1704
Droty MD, Dauskardt RH, Kant A, Ritchie RO (1995) Fracture of synthetic diamond. J Appl Phys 78(5):3083–3088
Evans A (1997) Design and life prediction issues for high-temperature engineering ceramics and their composites. Acta Mater 45(1):23–40
Evans A, Heuer A, Porter D (1997) The fracture toughness of ceramics. In 4th conference on fracture, Canada
Faes M, Valkenaers H, Vogeler F, Vleugels J, Ferraris E (2015) Extrusion-based 3D printing of ceramic components. Proc CIRP 28:76–81, ISSN 2212–8271
Fu Z, Schlier L, Travitzky N, Greil P (2013) Three-dimensional printing of SiSiC lattice truss structures. Mater Sci Eng A 560:851–856, ISSN 0921–5093
Giménez S, Van der Biest O, Vleugels J (2007) The role of chemical wear in machining iron based materials by PCD and PCBN super-hard tool materials. Diamond Relat Mater 16:435–445
Goel P, Khan ZA, Siddiquee AN, Gupta RK (2012) Influence of slab milling process parameters on surface integrity of HSLA: a multi-performance characteristics optimization. Int J Adv Manuf Technol 61(9–12):859–871

Habibi MK, Samaei AT, Gheshlaghi B, Lu J, Lu Y (2015) Asymmetric flexural behavior from bamboo's functionally graded hierarchical structure: underlying mechanisms. Acta Biomater 16(2015):178–186

He M, Hutchinson J (1989) Int J Solids Struct 25:1053–1067

Hutchinson J (1989) Mechanisms of toughening in ceramics. In Theoretical and applied mechanics, IUTAM. Elsevier Science Publishers B.V. North-Holland

Jager I, Fratzl P (2000) Mineralised collagen fibrils: a mechanical model with a staggered arrangement of mineral particles. Biophysics 79:1737–1746

Jeong-Ho K, Paulino G (2002) Mixed-mode fracture of orthotropic functionally graded materials using finite element and the modified crack closure method. Eng Fract Mech 69:1557–1586

Karambelasa G, Santhanama S, Wing ZN (2013) Strombus gigas inspired biomimetic ceramic composites via SHELL – sequential hierarchical engineered layer lamination. Ceram Int 39:1315–1325

Kennam et al (2015) High-temperature machining guide. Machining guides. www.kennametal.com. Accessed 05 Nov 2015

Khan U, May P, O'Neill A, Coleman J (2010) Development of stiff, strong, yet tough composites by the addition of solvent exfoliated graphene to polyurethane. Carbon 48(14):4035–4041

Lee JJW, Morris D, Constantino PJ, Lucas PW, Smith TM, Lawn BR (2010) Properties of tooth enamel in great apes. Acta Biomater 6(12):1742–7061. doi:10.1016/j.actbio.2010.07.023, ISSN 4560–4565

Li J, Shi X, Wang L, Liu F (2007) Synthesis of biomorphological mesoporous TiO2 templated by mimicking bamboo membrane in supercritical CO2. J Colloid Interface Sci 315(1):230–236

Li G, Li P, Yu Y, Jia X, Zhang S, Yang X, Ryu S (2008a) Novel carbon fiber/epoxy composite toughened by electrospun polysulfone nanofibers. Mater Lett 62:511–514

Li G, Li P, Zhang C, Yu Y, Liu H, Zhang S, Jia X, Yang X, Xue S (2008b) Inhomogeneous toughening of carbon fiber/epoxy composite using electrospun polysulfone nanofibrous membranes by in situ phase separation. Compos Sci Technol 68:987–994

Lin A, Meyers MA (2005) Growth and structure in abalone shell. Mater Sci Eng A 390:27–41

Lin S, Xiong D, Liu M, Bai S, Zhao X (2014) Thermophysical properties of SiC/Al composites with three dimensional interpenetrating network structure. Ceram Int 40:7539–7544

Magniez K, Chaffraix T, Fox B (2011) Toughening of a carbon-fibre composite using electrospun poly(hydroxyether of Bisphenol A) nanofibrous membranes through inverse phase separation and inter-domain etherification. Materials 4:1967–1984

McNamara D, Alveen P, Carolan D, Murphy N, Ivanković A (2015) Fracture toughness evaluation of polycrystalline diamond as a function of microstructure. Eng Fract Mech 143:1–16, ISSN 0013–7944

Mishnaevsky LJ (2005) Numerical experiments in the mesomechanics of materials. Darmstadt University of Technology, Germany

Morrell R, Danzer R, Supanic P, Harrer W, Puchegger S, Peterlik H (2010) Meso-scale mechanical testing methods for diamond composite materials. Int J Refract Met Hard Mater 28(4):508–515

Mortensen A, Suresh S (1997) Functionally graded metals and metal-ceramic composites. Int Mater Rev 42(3):85–116

Munch E, Launey ME, Alsem DH, Saiz E, Tomsia AP, Ritchie RO (2008) Tough, bio-inspired hybrid materials. Science 322:1516–1520

NanoSteel (2015) NanoSteel at Powder Met 2015. Powder Met (MPIF), San Diego, 17–20 May

Narutaki N, Yamane Y (1979) Tool wear and cutting temperature of cBN tools in machining of hardened steels. Ann ICRP 28(1):23–28

Nassif N, Pinna N, Gerhke N, Antonietti M et al (2005) Amorphous layer around aragonite platelets in nacre. Proc Natl Acad Sci USA 102:12653–12655

Neumann P (1969) Coarse slip model in fatigue. Acta Metall 17:1219–1225

Okamoto S, Nakazono Y, Otsuka K, Shimoitani Y, Takada J (2005) Mechanical properties of WC/Co cemented carbide with larger WC grain size. Mater Charact 55(4–5):281–287, ISSN 1044–5803
Oksman K, Craig C (1998) Mechanical properties and morphology of impact modified polypropylene-wood flour composites. J Appl Polym Sci 67:1503–1513
Petrovic M, Carolan D, Ivankovic A, Murphy N (2011) Role of rate and temperature on fracture and mechanical properties of PCD. Key Eng Mater 452(452–453):153–156
Rabiei R, Bekah S, Barthelat F (2010) Failure mode transition in nacre and bone-like materials. Acta Biomater 6:4081–4089
Raj R, Thompson L (1994) Design of the microstructural scale for optimum toughness in metallic composites. Acta Metall Mater 42(12):4135–4142
Ritchie R (1988) Mechanisms of fatigue crack propagation in metals, ceramics and composites: role of crack-tip shielding. Mater Sci Eng A103:15–28
Ritchie R (1999) Mechanisms of fatigue-crack propagation in ductile and brittle solids. Int J Fract 100:55–83
Ritchie RO (2011) The conflicts between strength and toughness. Nat Mater 10:817–822
Roe K, Siegmund T (2003) An irreversible cohesive zone model for interface fatigue crack growth simulation. Eng Fract Mech 70:209–232
Roether J, Baccaccin A (2005) Dispersion-reinforced glass and glass-ceramic matrix composites. In Handbook of ceramic composites, United Kingdom, Springer, p 554
Sandvik Hard Materials (2005) Cemented carbide, Sandvik new developments and applications. http://www2.sandvik.com/sandvik
Sarikaya M (2002) Biomimetics: nanomechanical design of materials through biology. In: ASCE engineering mechanics. Columbia University, New York
Scott D (2006) The history and impact of synthetic diamond cutters and diamond enhanced inserts on the oil and gas industry. Ind Diam Rev 66(1):48–55
Shao J-J, Vail TP, Wang Q-J, Jiang Y, Zhang X-L (2013) Anatomical references for tibial sagittal alignment in total knee arthroplasty: a comparison of three anatomical axes based on 3D reconstructed CT images. Chin Med J (Engl) 126(20):3840–3844
Shao Y, Zhao H-P, Feng X-Q, Gao H (2012) Discontinuous crack-bridging model for fracture toughness analysis of nacre. J Mech Phys Solids 60:1400–1419
Shum D, Hutchinson W (1990) On toughening by microcracks. Mech Mater 9:83–90
Song F, Bai YL (2003) Effects of nanostructures on the fracture strength of the interfaces in nacre. J Mater Res 18:1741–1744
Sowmya S, Bumgardener JD, Chennazhia KP, Naira SV, Jayakumar R (2013) Role of nanostructured biopolymers and bioceramics in enamel, dentin and periodontal tissue regeneration. Prog Polym Sci 38:1748–1772
Tan H, Wie Y (1998) Toughening mechanisms of nano-composite ceramics. Mech Mater 30:111–123
Torres-Sanchez C, Corney JR (2011) A novel manufacturing strategy for bio-inspired cellular structures. Int J Design Eng 4(1):5–22
Ural A, Krishnan VR, Papoulia KD (2009) A cohesive zone model for fatigue crack growth allowing for crack retardation. Int J Solids Struct 46:2453–2462
Walter M, Ravichandran G, Ortiz M (1997) Computational modelling of damage evolution in unidirectional fiber reinforced ceramic matrix composites. Comput Mech 20:192–198
Wang C, Huang Y, Zan Q, Guo H, Cai S (2000) Biomimetic structure design: a possible approach to change the brittleness of ceramics in nature. Mater Sci Eng C 11:9–12
Wang T, Dangsheng X, Tianle Z (2010) Preparation and wear behavior of carbon/epoxy resin composites with an interpenetrating network structure derived from natural sponge. Carbon 40:2435–2441

Wanga Y, Liu Z (2008) Tribological properties of high temperature self-lubrication metal ceramics with an interpenetrating network. Wear 265:1720–1726

Westraadt JE, Sigalas I, Neethling JH (2015) Characterisation of thermally degraded polycrystalline diamond. Int J Refract Met Hard Mater 48:286–292

Yun N, Won Y, Kim S (2004) Toughening of epoxy composite by dispersing polysulfone particle to form morphology spectrum. Polym Bull 52:365–372

Zhang Y, Sahasrabudhe H, Bandyopadhyay A (2015) Additive manufacturing of Ti-Si-N ceramic coatings on titanium. Appl Surf Sci 346(15):428–437, ISSN 0169–4332

Zimmermann M, Lahres M, Viens DV, Laube BL (1997) Investigations of the wear of cubic boron nitride cutting tools using Auger electron spectroscopy and X-ray analysis by EPMA. Wear 209(1–2):241–246, ISSN 0043–1648